

Multiresolution imaging of MEG cortical sources using an explicit piecewise model[☆]

Benoit Cottareau,^{a,b,*} Karim Jerbi,^a and Sylvain Baillet^a

^aCognitive Neuroscience and Brain Imaging Laboratory, CNRS UPR 640 LENA, University Pierre and Marie Curie-Paris6, Hôpital de la Salpêtrière, Paris, France

^bESME-Sudria College of Engineering, Ivry, France

Received 8 January 2007; revised 6 July 2007; accepted 16 July 2007
Available online 11 August 2007

Imaging neural generators from MEG magnetic fields is often considered as a compromise between computationally-reasonable methodology that usually yields poor spatial resolution on the one hand, and more sophisticated approaches on the other hand, potentially leading to intractable computational costs.

We approach the problem of obtaining well-resolved source images with unexcessive computation load with a multiresolution image model selection (MiMS) technique. The building blocks of the MiMS source model are parcels of the cortical surface which can be designed at multiple spatial resolutions with the combination of anatomical and functional priors. Computation charge is reduced owing to 1) compact parametric models of the activation of extended brain parcels using current multipole expansions and 2) the optimization of the generalized cross-validation error on image models, which is closed-form for the broad class of linear estimators of neural currents. Model selection can be complemented by any conventional imaging approach of neural currents restricted to the optimal image support obtained from MiMS.

The estimation of the location and spatial extent of brain activations is discussed and evaluated using extensive Monte-Carlo simulations. An experimental evaluation was conducted with MEG data from a somatotopic paradigm. Results show that MiMS is an efficient image model selection technique with robust performances at realistic noise levels.

© 2007 Elsevier Inc. All rights reserved.

Keywords: Electromagnetic brain imaging; MEG; Current multipole expansion; Multiresolution; Generalized cross-validation; Model selection; Optimization

[☆] Research supported by the French Ministry of Research: ACI New Interfaces of Mathematics and ACI Computational and Integrative Neuroscience.

* Corresponding author. Cognitive Neuroscience and Brain Imaging Laboratory, 47, boul. de l'hôpital, 75651 Paris Cedex 13, France.

E-mail address: benoit.cottareau@chups.jussieu.fr (B. Cottareau).

URL: <http://cogimage.dsi.cnrs.fr> (B. Cottareau).

Available online on ScienceDirect (www.sciencedirect.com).

Introduction

When MEG source estimation is approached as an image reconstruction problem (Baillet et al., 2001), the image source model is typically built from elementary sources such as current dipoles, which are distributed either within the entire 3D head volume or alternatively onto the individual cortical anatomy with orientations normal to the local cortical surface (Dale and Sereno, 1993). We note Γ the cortical envelope that sustains the source model and \mathcal{D} the set of n elementary cortical dipoles d_i , that sample Γ . We refer to $\mathcal{D} = \{d_i \in \Gamma, i \in [1, 2, \dots, n]\}$ as the global image support of neural currents.

The forward model of instantaneous data formation writes:

$$\mathbf{B} = \mathbf{G}\mathbf{J} + \boldsymbol{\epsilon}, \quad (1)$$

where \mathbf{B} is a matrix of m measurements on the MEG sensor array; \mathbf{J} are the unknown source amplitudes of all elementary sources in \mathcal{D} ; \mathbf{G} is the forward gain matrix that collects their forward fields sampled at the sensor array (Moshier et al., 1999); $\boldsymbol{\epsilon}$ is an additive nuisance term. The resulting imaging problem consists in deriving an inverse model for the amplitudes of the elemental current elements. In MEG imaging however, this inverse problem is cursed by severe underdetermination (i.e. $n \gg m$) and has fundamentally no unique solution (Hämäläinen et al., 1993). Conventional addresses to this issue stem from the concept of regularization which classically reduces to complementing the image source model with additional priors or constraints (Demoment, 1989; Baillet et al., 2001; Auranen et al., 2005). Such complementary information may take many faces in MEG and EEG (electroencephalography) source imaging, though generally reduces to considering that the current distribution is either spatially smooth or sparse focal.

Smoothness is readily enforced by the broad class of minimum-norm priors which may apply either directly to the amplitude of currents (Wang et al., 1992) or to some of their low-order spatial derivatives (e.g. gradient or Laplacian; Pascual-Marqui et al., 1994). These current estimates are generally robust to a reasonable amount of nuisance in the data and approximations in the compu-

tation of \mathbf{G} (Wagner et al., 2004). They are also fast to compute because the estimate is unique and linear in the data, but they suffer by construction from exaggerated poor spatial resolution, which bridles their development and murk the appraisal of the corresponding current estimates. Classical sparse focal image models have been introduced as a response to these limitations and are reviewed in (Baillet et al., 2001). However, selecting a particular class of image models to ensure sparsity in the estimated distribution of currents is certainly as arbitrary as preferring either one of the smooth image models instead.

Hence, while there is a long tradition of considering inverse modelling as an optimization problem i.e. designate the solution to an inverse problem as the source model corresponding to the putative global maximum of some adequacy functional we are facing the situation that the number of equally-satisfactory image models is just too large to depart from complete arbitrariness. Such an issue is general to the resolution of severely ill-posed inverse problems, and has triggered a steady paradigm shift from mere model optimization to model selection (Knösche et al., 1998; Waldorp et al., 2002; Tarantola, 2006).

As for regularization, model selection can be naturally approached with the Bayesian theory of probability where multiple levels of inferences can be achieved, unconditional on the image model assumed (Trujillo-Barreto et al., 2004). These recent developments extend the approaches to model optimization in the Bayesian framework that were previously introduced for MEG in (Baillet and Garnero, 1997; Phillips et al., 1997). Though very elegant and promising, exact Bayesian inference for model selection is computationally demanding (Sato et al., 2004; Daunizeau et al., 2005; Phillips et al., 2005; Friston et al., 2006), which may necessitate to reduce the number of free parameters in the image model (e.g. the number n of elementary sources; Schmidt et al., 1999).

Alternatives to Bayesian model selection from sparse-focal image priors have been empirically approached with the combination of iterative optimization with multiresolution image models. In this context, the image support \mathcal{D} is altered during the global estimation procedure by removing some brain regions from the image model when moving to the next spatial resolution (Gorodnitsky et al., 1995; David and Garnero, 2002; Liu et al., 2005). This leads to some necessary limitation on the number of free parameters to be estimated at each iteration step, hence the need to design economical model of the entire distribution of cortical currents. Choosing a simple (i.e. low-dimensional) model for extended regional brain activity e.g. (Gavit et al., 2001), where an elementary current dipole would account for a larger, spatially-extended activity of a cortical parcel is exposed to the risk of yielding a global source model of limited predictive power. Conversely, advanced regional source models as in (Moran et al., 2005; Daunizeau et al., 2005) may require a larger number of parameters that may reduce their practice to image supports that significantly depart from the intricate cortical geometry.

In this context, this article introduces a new framework for empirical multiresolution image model selection (MiMS) in MEG. We suggest the building blocks of the image models at various spatial resolutions be parcels of the cortical surface, thereby explicitly enforcing the prior on the sparse focal nature of the distribution of cortical currents on a short time segment. Cortical parcellation is achieved conditionally to the homogenous distribution of surface areas across parcels at each spatial resolution k , with additional priors from geometrical or even atlas-based features of

the cortical envelope (Piecewise modelling of the source image section). Efficient and compact parametric modelling of distributed currents within each parcel is achieved using their equivalent current multipole expansions (CME, Modelling neural currents at the regional scale section).

Model quality at each spatial resolution is evaluated according to the general cross-validation (GCV) error principle. This is detailed in the Model selection section where we also discuss how GCV error can be analytically – hence rapidly – evaluated in practice.

Rather than formulating this procedure in the Bayesian framework – where the elaboration of some of the marginal distributions on priors and related multilevel inference may be rather intricate – we have adopted the dual empirical frequentist world-view by implicitly sampling the posterior distributions of the image model using a multistart estimation procedure from multiple initial conditions. The MiMS approach yields an image model for a given data segment which may not be defined at the finest possible spatial resolution. We further derive from this procedure the empirical estimate of the probability for a given elementary dipole d_i of the global image support \mathcal{D} of being effectively active (A posteriori classification of elementary sources and estimation of neural currents section).

Following a similar approach as Mattout et al. (2005), the application of MiMS is illustrated in the A posteriori classification of elementary sources and estimation of neural currents section where the resulting map of probability-like coefficients is thresholded – to yield a subset of \mathcal{D} as the final image support model – and optionally acts as intrinsic functional priors when coupled to an imaging estimate of cortical currents. This latter approach will be exemplified with the association of MiMS to a weighted minimum-norm estimate (WMNE) of MEG sources, hence the MiMS WMNE acronym.

The technique is extensively evaluated on Monte-Carlo experiments, from which we discuss on the recovery of crucial parameters of activated brain regions such as location and spatial extent in the Monte-Carlo experiments section.

The evaluation is completed by the analysis of real MEG data from a paradigm on somesthetic mapping of hand fingers (Illustrative example on real data: somesthetic mapping of hand fingers section).

Methods

Rationale and methodological overview

We concisely review in this Section the multiple steps taken in the MiMS technique before they are further detailed in following subsections.

Extensive experimental evidences from e.g. functional Magnetic Resonance Imaging (fMRI) report on the regional sparse focal nature of instantaneous stimulus-evoked cortical activity. Further, neural sources of MEG and EEG are usually considered to be distributed in regions extending up to a few cm^2 (Tao et al., 2005; Murakami and Okada, 2006).

This sparse focal nature of neural currents at the regional level may be introduced explicitly in the image source model considered in the resolution of the associated inverse problem (Baillet and Garnero, 1997; Phillips et al., 1997). Here we further develop this approach in a multiresolution framework by considering parcels of the cortical surface envelope as building blocks of the image source model.

Let \mathcal{M}_k denote the image source model at spatial resolution k . This model predicts that instantaneous brain activity consists of a collection of n_c cortical parcels:

$$\mathcal{M}_k = \{\mathcal{C}_j^k, j \in [1, 2, \dots, n_c]\} \subset \Gamma. \quad (2)$$

In practice, each cortical parcel \mathcal{C}_j^k consists of a contiguous set of elemental dipoles from the global image source model \mathcal{D} .

In the very specific context of multiresolution image modelling, increasing the spatial resolution from k to $k+1$ implies decreasing the typical surface area of parcels in \mathcal{M}_{k+1} . This would induce the uncontrolled increase of n_c with k – hence of the number of unknowns in the image source model – if \mathcal{M}_k were supposed to sample the entire cortical manifold Γ .

Consequently, we assume that as spatial resolution increases, the support of the image source model does not cover the entire cortical manifold Γ anymore and that n_c is constant and does not depend on k . This may be achieved by discarding one of the parcels in \mathcal{M}_k to form \mathcal{M}_{k+1} as a set of n_c new and smaller cortical parcels. Hence, we define \mathcal{D}_k as the support of the image source model at spatial resolution k , which is a subset of elemental sources originally available in \mathcal{D} .

We further define $\mathcal{D}_1 = \mathcal{D}$ and k_{\max} , the finest spatial resolution where all parcels in $\mathcal{M}_{k_{\max}}$ consist of a single elementary dipole (hence $\text{card}(\mathcal{D}_{k_{\max}}) = n_c$).

Identifying which cortical parcel will be discarded from \mathcal{M}_k before moving to resolution $k+1$ yields some issues in model design and selection that are addressed as follows:

- (1) *Design of an image source model at resolution k* : the piecewise image model \mathcal{M}_k is designed from the set of elemental sources available in \mathcal{D}_k ;
- (2) *Model selection*: exhaustively evaluate the GCV error of all n_c sub-models of \mathcal{M}_k consisting in alternatively removing one of its n_c parcels. The elementary dipoles of the cortical parcel which, when removed from \mathcal{M}_k , yields the submodel with the least GCV error are removed from \mathcal{D}_k to yield \mathcal{D}_{k+1} , the support of the image source model at the next spatial resolution $k+1$.

This multiresolution image model selection (MiMS) is conducted iteratively until the finest possible spatial resolution k_{\max} is reached. The best image source model in the least GCV error sense is defined retrospectively as \mathcal{M}_{k^*} .

Uncertainty on the determination of k^* – that is on the final model selection – is empirically inferred by restarting the entire procedure by sampling multiple designs for the initial piecewise image model \mathcal{M}_1 .

As an immediate benefit, the MiMS results in a score map \mathbf{W} of the empirical probability of any elemental source $d_i \in \mathcal{D}$ to belong to the final image source model (A posteriori classification of elementary sources and estimation of neural currents section).

This map may either be thresholded to classify sources in \mathcal{D} as either being *active* or *non-active* and/or directly passed as intrinsic prior weights to a subsequent imaging procedure to estimate neural currents (Mattout et al., 2005). This will be illustrated in the Results section.

We now proceed to the detailed description of the technical aspects of each of these steps.

Piecewise modelling of the source image

At each spatial resolution k , the set of available elemental dipoles \mathcal{D}_k is paved with n_c non-overlapping cortical parcels \mathcal{C}_j^k obtained from a region-growing procedure with neuroanatomical priors.

The rationale supporting this approach anticipates that new neuroanatomical atlases (Mazziotta et al., 2001; Toga et al., 2006) and the development of high-field MRI will help unveil the interplay between the structural morphology and functional significance of many brain regions, thereby contributing to new functional imaging models with increasingly pertinent anatomic-functional and neuro-architectural priors.

As a proof of concept, the atlas of Brodmann areas delineated on the Colin27 image set from the Montreal Neurological Institute (MNI) was back-projected with a nearest-neighbor approach onto the individual cortical anatomy of the subjects involved in this study, once all MRI scans were co-registered in the MNI normalized referential with affine transformations (BrainStorm toolbox, <http://neuroimage.usc.edu/brainstorm>).

Cortical circumvolutions were also considered as additional guidelines to parcellation at a more local scale, by favoring minimal curvature within a given parcel. The cortical manifold Γ was extracted from T1-weighted MRI axial scans ($1 \times 1 \times 1.5$ mm voxel size) and triangulated using the automatic pipeline of processes from The Anatomist software available in the brainVISA environment (<http://brainvisa.info>). The global image support \mathcal{D} for MEG source modelling was obtained from the resulting tessellation of the cortical surface by distributing a current dipole at each node of the corresponding triangulation, with its orientation normal to the local cortical surface.

The cortical surface was subsequently automatically segmented into crest zones, i.e. regions where surface curvature is locally homogenous. Crest zones were obtained from a region-growing process using crest lines as elementary skeletons (Stylianou and Farin, 2004). Crest line are sets of points of Γ where surface curvature is flat (Stylianou and Farin, 2003). In practice, cortical crest zones grow from the gyral crowns of the cortex and meet at sulcal fundi (Figs. 1d–f). This approach yields an extension to surface manifolds of existing volumic, voxel-based, parcellation techniques (Flandin et al., 2002).

These two pieces of priors (Brodmann and crest zones) were combined at every spatial resolution k to build the cortical parcels of \mathcal{M}_k with the additional constraint that the distribution of parcel surface areas should be uniform. Let A_k denote the average surface area of a parcel at resolution k :

$$A_k = \frac{\mathcal{S}(\mathcal{D}_k)}{n_c}, \quad (3)$$

where $\mathcal{S}(\mathcal{D}_k)$ is the total surface area of the image support at resolution k . The region-growing process is seeded randomly at an elemental dipole source $d_i \in \mathcal{D}_k$ and yields all \mathcal{C}_j^k parcels in \mathcal{M}_k with the following constraints:

- (1) $\mathcal{S}(\mathcal{C}_j^k) \sim A_k, \forall j \in [1, n_c]$;
- (2) dipoles in \mathcal{C}_j^k belong to neighboring regional areas. Here, a regional area is defined as the intersection between a Brodmann area and a crest zone.

When all elementary sources from a regional area have been included in a given parcel \mathcal{C}_j^k and while $\mathcal{S}(\mathcal{C}_j^k) < A_k$, region growth extends to the next available contiguous regional area.

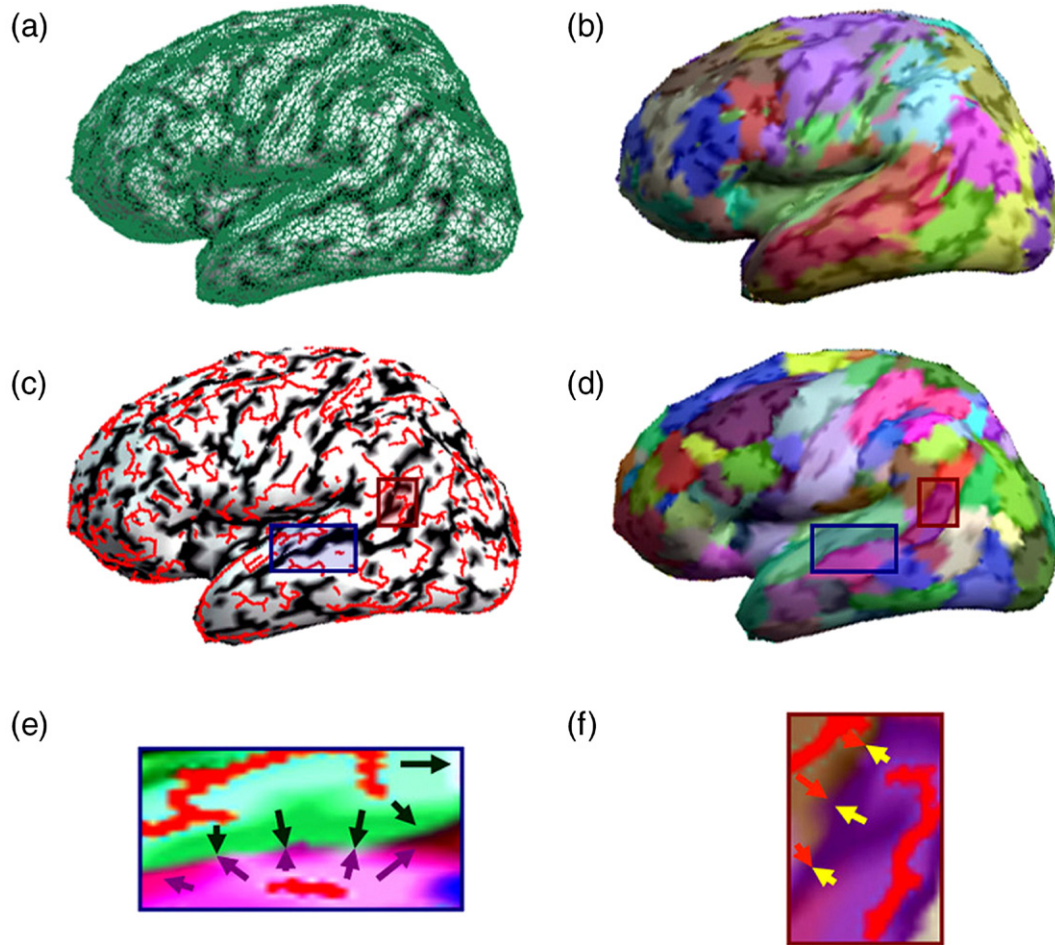


Fig. 1. (a) The global image support: lateral view of a smoothed tessellated cortical envelop with $\sim 10,000$ vertices; (b) the estimation of Brodmann areas following affine registration with the MNI atlas; (c) the crest lines (in red) extracted automatically from the cortical surface envelope using a method adapted from Stylianou and Farin (2004). In this example, about 100 crest lines were identified automatically on each hemisphere; (d) exemplifies the obtention of crest zones of homogeneous curvature from the growth about crest lines. As each line acts as an elemental skeleton to a crest zone, the final segmentation contained approximatively 200 crest regions over the entire cortex. See (e) and (f) for local magnifications: arrows indicate how crest zones grow from skeletal crest lines using the neighborhood of the sources belonging to each line.

When $\mathcal{S}(\mathcal{C}_j^k)$ reaches A_k , another dipole seed is chosen randomly from the remaining elemental dipoles in \mathcal{D}_k and the process iterates until there is no elemental source left available.

This parcellation procedure is automatic and fast: it takes about 10 s to segment the entire cortical surface in 20 parcels of 100 cm^2 on a conventional workstation (3 GHz-Pentium4, 1 GB RAM) using Matlab (The Mathworks, Natick, MA). We have found this technique yields satisfactory results in terms of homogeneity in the distribution of parcel surface areas (see Fig. 2 for an illustration).

Modelling neural currents at the regional scale

A compact parametric model of neural currents sustained by every parcel \mathcal{C}_j^k was subsequently designed. At coarser resolutions, a single equivalent current dipole (ECD) is a poor model for regional activations extending above 5 cm^2 (de Munck et al., 1988; Jerbi et al., 2002). Specific source models for spatially-extended cortical currents have been proposed recently (David and Garnero,

2002), but these latter are often disconnected from the physics of MEG and rather result from pragmatic approaches to the reduction in the number of unknowns in the source imaging problem. Another straightforward empirical model for extended sources would consist of a truncated principal component analysis (PCA) of the MEG gain submatrix made from the forward fields of the elementary dipoles in a given parcel \mathcal{C}_j^k (Limpiti et al., 2006), or using any set of local basis functions. This approach questions the choice for a threshold in the truncation of the PCA or for the total dimension of the local basis functions under consideration. These values could be estimated explicitly from the data – hereby severely aggravating the computation load – and would also implicitly depend on multiple characteristics of the regional source that are yet not fully understood.

Current multipolar expansions (CME) stem from the very principles of the generation of magnetic fields and unified formulations have been recently derived for MEG (Nolte and Curio, 2000; Jerbi et al., 2002). Jerbi et al. (2004) further demonstrated that CME models up to the quadrupolar order outperformed the ECD for both focal and spatially-extended neural activity, while considerably

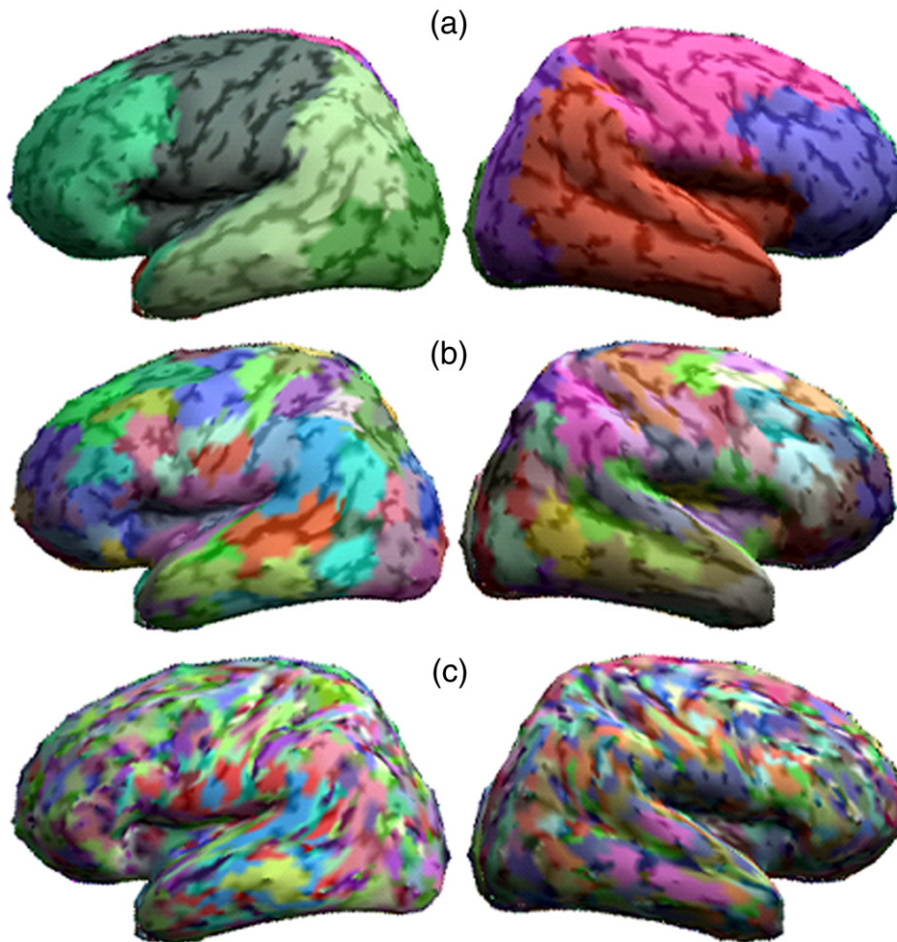


Fig. 2. Illustrative results from cortical parcellation procedure. Examples shown are with (a) 20, (b) 200 and (c) 2000 parcels. The corresponding average (resp. standard deviation) of the resulting parcel surface areas are (a) 100 (resp. 24) cm^2 , (b) 10 (resp. 1.8) cm^2 and (c) 1 (resp. 0.2) cm^2 , which indicates a satisfactory degree of homogeneity in their distribution.

keeping a small fixed number of parameters to model regional currents.

Given the intricate circumvolutions of the cortex, a minimum of 10,000 nodes are often considered as necessary to achieve the proper spatial sampling of its surface for MEG source imaging. This yields a minimum source density of 4 dipoles/ cm^2 (on a realistic cortex tessellation of about 2000 cm^2), hence 20 dipole amplitude parameters would be necessary to model the current flows sustained by 5 cm^2 of cortex in a basic source imaging approach. The 7 moments of the corresponding quadrupolar CME model demonstrated equivalent modelling abilities provided that the distribution of surfacic currents is locally smooth (Jerbi et al., 2004).

Therefore, the equivalent CME of each parcel $\mathcal{C}_j^k \in \mathcal{M}_k$ is computed explicitly about its centroid (Jerbi et al., 2004). The general forward modelling Eq. (1) may then be rewritten under the following compact form:

$$\mathbf{B} = \bar{\mathbf{G}}_k \bar{\mathbf{m}}_k + \epsilon, \quad (4)$$

where $\bar{\mathbf{G}}_k$ is the $m \times n_p$ CME gain matrix of the piecewise image source model \mathcal{M}_k at spatial resolution k , with $n_p = n_c \times 7$, the total number of unknowns in \mathcal{M}_k , which does not depend on k (see Rationale and methodological overview section). $\bar{\mathbf{m}}_k$ is an array of

height n_p gathering the CME moments of all parcels in the model for each time instant.

We note that CME models have been extensively studied in MEG and have been derived in EEG only just recently (Dassios, in press). Hence we restrict this article to MEG source modelling but we anticipate the maturation of EEG CME source models will permit the use of MiMS in a similar manner.

For the resolution of (4) to be numerically tractable and fast at all spatial resolutions, we chose to keep the total number of unknown parameters n_p down to $n_p \sim m$, the number of instantaneous measurements, hence the total number of parcels $n_c \sim m/7$ is indeed independent of the spatial resolution k .

Model selection

As spatial resolution increases from k to $k+1$, the building blocks of \mathcal{M}_{k+1} become smaller, with $A_{k+1} < A_k$. As the total number of model parameters is kept constant across spatial resolutions (see Modelling neural currents at the regional scale section), one parcel is removed from \mathcal{M}_k to yield \mathcal{D}_{k+1} . Choosing which of the n_c parcels needs to be removed is a model selection process that we shall now detail.

Let us define $\mathcal{M}_{k|j}$, a submodel of \mathcal{M}_k , which consists of all parcels in \mathcal{M}_k but \mathcal{C}_j^k , that is:

$$\mathcal{M}_{k|j} = \{\mathcal{C}_p^k, p \in [1, 2, \dots, n_c], p \neq j\}. \quad (5)$$

The parcel to be removed from \mathcal{M}_k is the one which corresponding submodel minimizes the leave-one-out generalized cross-validation (GCV) error. This criterion ensures the best similarity of the respective predictive powers between the two consecutive models \mathcal{M}_k and \mathcal{M}_{k+1} (see e.g. Reeves and Mersereau, 1992) and has been adopted in a considerable number of estimation problems, including other applications of multiresolution imaging (Nguyen et al., 2001a).

In practice, the GCV error ε_j^k of each of the n_c submodels $\mathcal{M}_{k|j}$ is sequentially evaluated under the assumption that the corresponding CME moments from (4) are derived from the following weighted minimum-norm estimate:

$$\hat{\mathbf{m}}_{k|j} = \bar{\mathbf{G}}_{k|j}^t [\bar{\mathbf{G}}_{k|j} \bar{\mathbf{G}}_{k|j}^t + \lambda \bar{\mathbf{C}}_k^{-1}]^{-1} \mathbf{B}, \quad (6)$$

where $\bar{\mathbf{G}}_{k|j}$ (resp. $\hat{\mathbf{m}}_{k|j}$) denotes the CME gain matrix $\bar{\mathbf{G}}_k$ (resp. the estimate of CME moments $\hat{\mathbf{m}}_k$) deprived of the 7 columns (resp. moments) of the CME model of \mathcal{C}_j^k ; λ is a scalar regularization parameter and $\bar{\mathbf{C}}_k$ is a regularizing spatial covariance prior on CME moments. This assumption insures fundamental benefits on the closed-form estimation of ε_j^k as we shall see below. Following the directions described in Jerbi et al. (2004), a database of sample estimates of $\bar{\mathbf{C}}_k$ can be built a priori and stored to disk from each individual brain anatomy of the subjects involved in a given study. The estimation of $\bar{\mathbf{C}}_k$ was obtained from source samples consisting of 250 regional sources with sizes within the [1,10] cm² range and 100 pAm.mm⁻² dipole moment density within cortical parcels spanning 10 bins of typical surface areas A_k in the [1,100] cm² range.

A major benefit from the minimal GCV error criterion is that ε_j^k is closed form when the estimate of model parameters is linear as in (6); see Nguyen et al. (2001b) for demonstration:

$$\varepsilon_j^k(\lambda) = \frac{\|(\bar{\mathbf{G}}_{k|j} \bar{\mathbf{G}}_{k|j}^t + \lambda_j^k \bar{\mathbf{C}}_k^{-1})^{-1} \mathbf{B}\|}{\text{trace}((\bar{\mathbf{G}}_{k|j} \bar{\mathbf{G}}_{k|j}^t + \lambda_j^k \bar{\mathbf{C}}_k^{-1})^{-1})} \quad (7)$$

We selected λ_j^k as:

$$\lambda_j^k = \underset{\lambda \in [\sigma_m, \sigma_M]}{\text{argmin}} \varepsilon_j^k(\lambda). \quad (8)$$

from an exhaustive search on 1,000 bins, where σ_m (resp. σ_M) is the smallest (resp. largest) singular value of $\bar{\mathbf{G}}_{k|j} \bar{\mathbf{C}}_k^{-1}$, with $\bar{\mathbf{C}}_k^{-1}$ the left part of the Cholesky decomposition of $\bar{\mathbf{C}}_k^{-1}$ (Wahba, 1990). Iterations on k are pursued exhaustively until the finest spatial resolution k_{\max} as defined in the Rationale and methodological overview section is reached. The optimal model \mathcal{M}_{k^*} in the least GCV-error sense is obtained by retrospectively identifying k^* as:

$$k^* = \underset{k}{\text{argmin}} \varepsilon_k, \quad (9)$$

where

$$\varepsilon_k = \min_j \varepsilon_j^k. \quad (10)$$

The optimal model depends on the initial image source model \mathcal{M}_1 which was designed from the arbitrary selection of a seed point to the cortical parcellation process at $k=1$.

The posterior uncertainty on the optimal image source model can be sampled empirically by L random initial conditions (e.g. by randomly changing the seed point of the cortical parcellation at $k=1$).

This results in a posterior empirical estimate of whether any elemental dipole source $d_i \in \mathcal{D}$ is likely to be activated during the analyzed data segment. Indeed, an activation coefficient is computed from the accuracy score w_i attributed to each elemental dipole source d_i and is defined as:

$$\forall d_i \in \mathcal{D}, w_i = \sum_{l=1}^L w_i^l, \quad (11)$$

with

$$w_i^l = \begin{cases} 1/\varepsilon_{k^*} & \text{if } d_i \in \mathcal{M}_{k^*} \\ 0 & \text{otherwise} \end{cases}.$$

This results in a map \mathbf{W} of the empirical probability values that elemental dipoles in \mathcal{D} be activated:

$$\mathbf{W} = \{\bar{w}_i, d_i \in \mathcal{D}\}, \quad (12)$$

where

$$\bar{w}_i = \frac{w_i}{\max_i(w_i)} \in [0, 1]. \quad (13)$$

A posteriori classification of elementary sources and estimation of neural currents

Empirical probability values in \mathbf{W} may be passed as intrinsic priors to any imaging procedure defined on the entire set of elementary cortical dipoles \mathcal{D} as suggested by Mattout et al. (2005), but here with a different approach. Following these authors steps, \mathbf{W} may also be thresholded to discriminate between active and non-active elementary dipoles. We define Γ_A (resp. Γ_{NA}) the set of active (resp. non-active) elementary sources.

A K -means classifier with random initialization is applied to the \mathbf{W} map (with $K=2$ classes) to discriminate between Γ_A and Γ_{NA} . Finally, the elementary current dipoles belonging to Γ_A yield the optimal image support $\mathcal{D}_{\text{MiMS}}$ obtained from the MiMS multi-resolution image model selection.

The MiMS image support may be naturally coupled to the corresponding activation probabilities in \mathbf{W} to inform any imaging estimator of neural currents. We exemplify this paired estimation of neural currents with the MiMS WMNE estimate of neural currents, $\hat{\mathbf{J}}_{\text{MiMS}}$:

$$\hat{\mathbf{J}}_{\text{MiMS}} = \mathbf{G}_{\text{MiMS}}^t (\mathbf{G}_{\text{MiMS}} \mathbf{G}_{\text{MiMS}}^t + \lambda \mathbf{W}_{\text{MiMS}}^{-1})^{-1} \mathbf{B}, \quad (14)$$

where \mathbf{G}_{MiMS} is the gain matrix of the set of elemental dipoles in $\mathcal{D}_{\text{MiMS}}$;

$$\mathbf{W}_{\text{MiMS}} = \{W(i), i \in \mathcal{D}_{\text{MiMS}}\}, \quad (15)$$

and λ takes the optimal value in the least GCV-error sense as defined in (8).

Results

The performances of the MiMS procedure were extensively evaluated with Monte-Carlo experiments on the influence of the number and size of active brain regions. Sensitivity to increasing noise levels was also evaluated. This section closes with the evaluation of MiMS and MiMS WMNE on a real MEG data set.

Data processing, forward modelling and visualization were developed with BrainStorm in a spherical head geometry using the 151-channel whole-head MEG array of axial gradiometers from the CTF Omega system from VSM MedTech (Coquitlam, BC, Canada).

Let us first begin with an illustrative example of the MiMS procedure.

The MiMS illustrated

Three 10 cm² brain regions were virtually activated with a uniform current distribution as displayed Fig. 6a. Independent and identically-distributed (IID) Gaussian noise samples with zero mean were added to the simulated data. The noise level was set to 20% as defined by the ratio between the Frobenius norm of the noise across MEG sensors to the Frobenius norm of the signal due to the activated brain regions.

Fig. 3 plots the GCV error ε_k obtained from Eq. (10) versus spatial resolution k during an exhaustive exploration of all spatial resolutions with the MiMS.

The empirical probability map \mathbf{W} is obtained from Eq. (12) and is shown Fig. 4.

Active elemental dipoles in \mathcal{D} are selected from this map (see A posteriori classification of elementary sources and estimation of

neural currents section and Fig. 5), yielding the MiMS image support $\mathcal{D}_{\text{MiMS}}$ (Fig. 6c) which when combined with \mathbf{W} may be used as a prior to any imaging estimation of the amplitudes of the elemental dipoles in the model, as illustrated Fig. 6d with the MiMS WMNE approach.

Monte-Carlo experiments

Evaluation procedure

Numerical Monte-Carlo simulations were performed to evaluate the multiresolution imaging approach respectively to the effects of the size and number of active regions.

250 Monte-Carlo trials were generated by simulating the simultaneous activation of 1 and 3 regions with identical surfaces areas ranging from 1 to 10 cm². Dipole amplitudes within a simulated active area were adjusted to ensure a surface current density of 100 pAm.mm⁻². Additive Gaussian noise was applied to the modelled data, again with a noise level of 20%.

$L=30$ – see Appendix B for a discussion on the choice of this value – samples of random initial conditions were used to obtain the MiMS image models. The MiMS procedure was programmed with Matlab and took about 1 min per Monte-Carlo trial on a conventional workstation (3 GHz-Pentium4, 1 GB RAM) for a cortical tessellation with 10,000 vertices.

Detection performances of image models: number and extension of active regions, and influence of noise

The performances of the MiMS were assessed with Receiver Operating Characteristics (ROC) analysis (Kay, 1993; Metz, 1998; Grova et al., 2006) and complemented with those from MiMS WMNE. The corresponding estimated source maps were thresholded at variable cutoff values β , to obtain the sample estimates

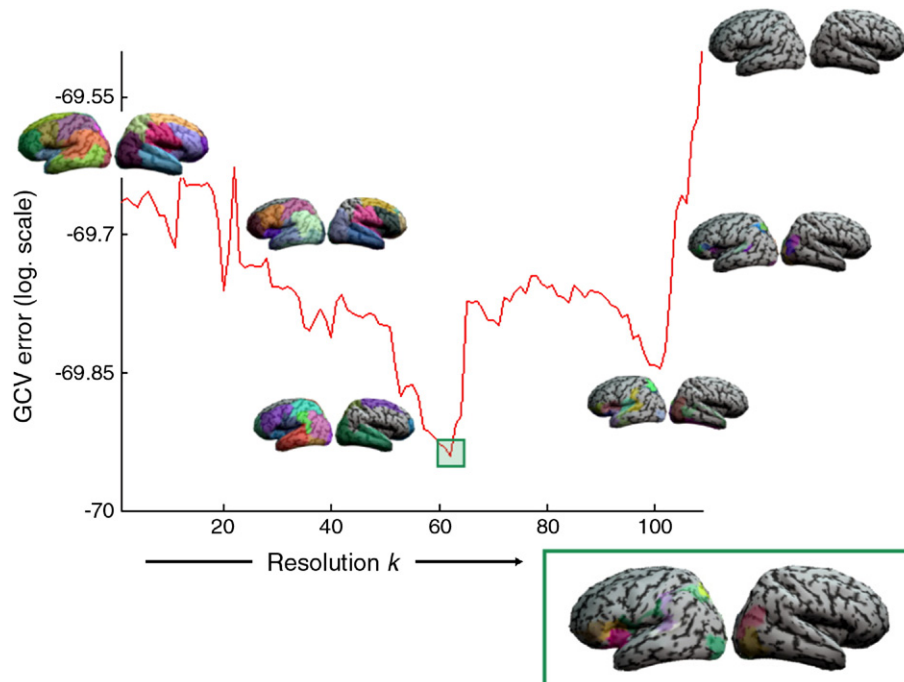


Fig. 3. GCV error ε_k vs. spatial resolution k in semilog scale. A selection of image source models \mathcal{M}_k are shown with their associated cortical parcels. Here, the global minimum of ε_k is reached for $k^*=62$ and the corresponding imaging model \mathcal{M}_{k^*} is magnified in the green boxplot.

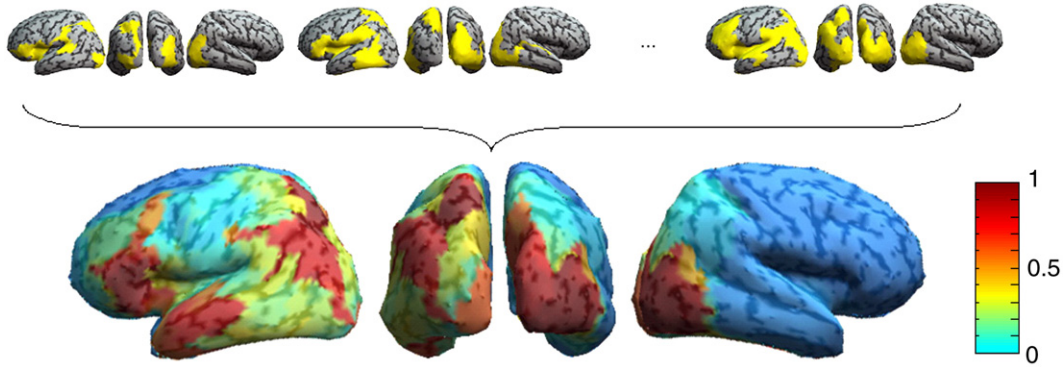


Fig. 4. The probabilistic map \mathbf{W} illustrated. Multiple samples of optimal models \mathcal{M}_{k^*} obtained from the empirical posterior evaluation of model uncertainty (top row). The normalized cumulative accuracy scores yield \mathbf{W} , the map of empirical probability of activation \bar{w}_i for every elemental dipole $d_i \in \mathcal{D}$ (bottom row).

of the threshold-dependent sensitivity $\mathcal{S}_e(\beta)$ and specificity $\mathcal{S}_p(\beta)$ of the source estimate following the conventional definitions:

$$\mathcal{S}_e(\beta) = \frac{\text{TP}(\beta)}{\text{TP}(\beta) + \text{FN}(\beta)}$$

$$\mathcal{S}_p(\beta) = \frac{\text{TN}(\beta)}{\text{TN}(\beta) + \text{FP}(\beta)}, \quad (16)$$

where TP, FP, TN and FN are the amounts of true positive, false positive, true negative and false negative detection rates for a cutoff value of β , respectively (see Appendix A for details).

ROC curves were obtained by plotting $\mathcal{S}_e(\beta)$ against $1 - \mathcal{S}_p(\beta)$. The area under the curve (AUC) was computed for each ROC curve as an index of the specificity-sensitivity compromise of the corresponding source models. Figs. 7 and 8 display the AUC indices from the Monte-Carlo trials when 1 and 3 regions are simultaneously active respectively.

Results show that the performances of conventional WMNE degrade with the increasing number of active regional sources and also with increasing surface areas, while the MiMS and MiMS

WMNE yield significantly better performances ($p < 0.01$, Kolmogorov–Smirnov test).

To study the specific influence of noise in the data on the detection performances of the image models, simulations of 50 source sets of 3 active 10 cm² regions were run at various noise levels: 0%, 5%, 10%, 15% and 20%. Fig. 9 plots the corresponding AUC against noise levels for 3 image models: WMNE, MiMS and MiMS WMNE.

The conventional WMNE model was clearly outperformed by the MiMS and the MiMS WMNE image models in terms of AUC values ($p < 0.01$, Kolmogorov–Smirnov test), which were always found above 0.85 for these latter, even at high noise levels.

In conclusion, the MiMS source models are robust to multiple simultaneous activations of brain regions over a broad range of surface areas. The image model is resistant to increasing noise levels, as no significant degradation of the performances was noticed up to 20% noise in the data.

On the estimation of the spatial extent of activations

We further questioned whether the MiMS-based image models would recover the spatial extent of the activated brain regions as this would yield a crucial functional marker of major brain processes such as e.g. plasticity and learning. The surface areas sampled by the MiMS image supports $\mathcal{D}_{\text{MiMS}}$ were directly compared to the true simulated surface areas of the Monte-Carlo experiments with one activated source, as described in the Monte-Carlo experiments section with 20% noise level. For the specific case of MiMS WMNE, the source amplitudes were thresholded using the cut-off value that produced the best compromise in sensitivity and specificity as revealed from the ROC analysis curves in the Evaluation procedure section.

Fig. 10 shows the plots of the true vs. estimated spatial extent of activated regions. Equations from linear regression models indicate that the MiMS strongly overestimates the spatial extent of activated sources, though with very significantly-correlated estimates ($r = 0.59$, $p < 10^{-10}$). Correlation improves dramatically with the coupled MiMS WMNE approach ($r = 0.74$, $p < 10^{-10}$) with a strong decrease of the overestimation of the true spatial extent of activations.

Sensitivity of the estimation of the active surface extent to noise was also investigated by Monte-Carlo simulations of 3 10 cm² regions with noise levels ranging up to 20% of the signal level, as in the Detection performances of image models: number and extension of active regions, and influence of noise section. Fig. 11 shows

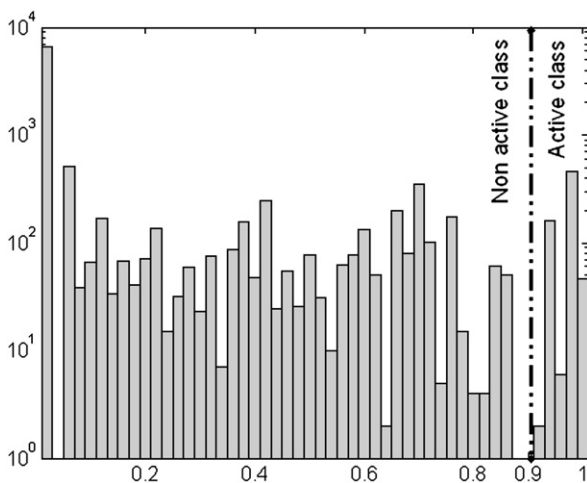


Fig. 5. Active vs. non-active source classification. Histogram of the empirical probability values in \mathbf{W} . A two-class K -means algorithm yields a threshold (here 0.9) to discriminate between active and non-active elemental sources.

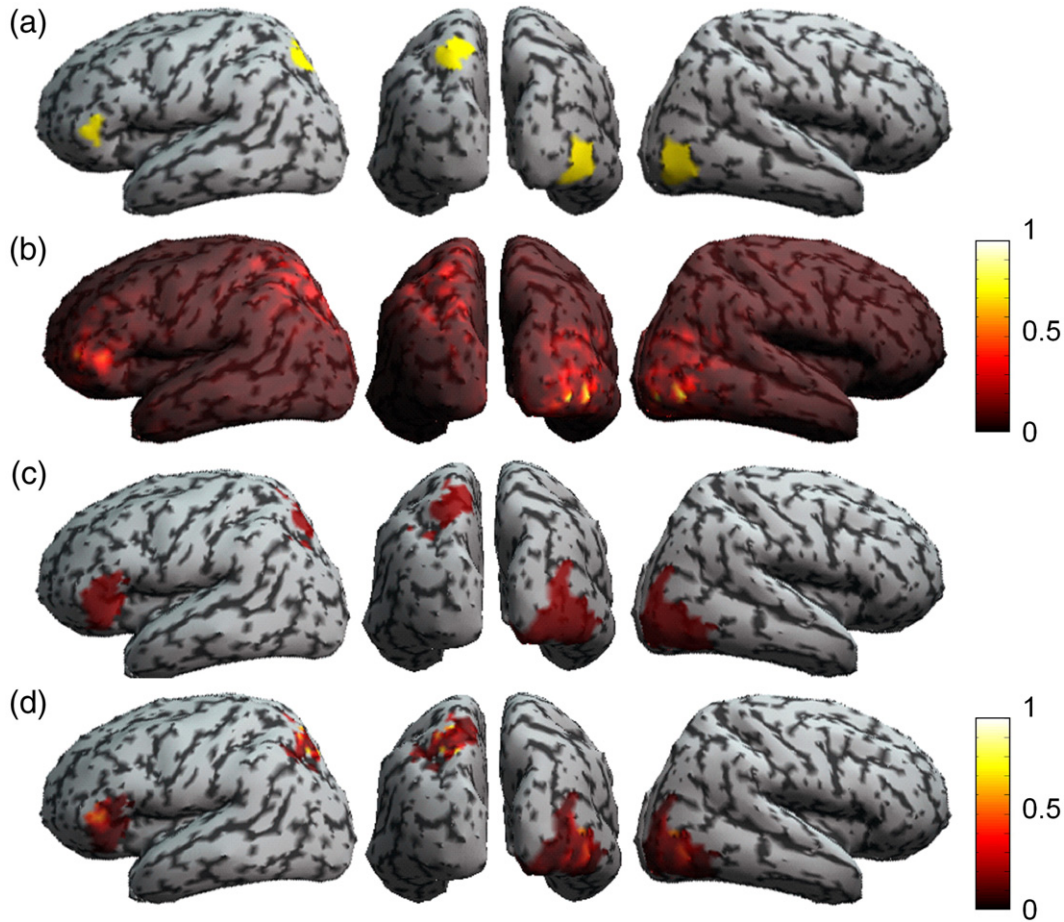


Fig. 6. Conventional WMNE vs. MiMS WMNE. (a) The original set of 3 activated parcels of 10 cm² each; (b) WMNE image estimate (in normalized units); (c) the optimal MiMS image support $\mathcal{D}_{\text{MiMS}}$ and (d) the corresponding MiMS WMNE estimation of neural currents (also in normalized units).

the average total surface area detected as being activated with the MiMS image model against increasing noise level. Note that the true total active surface areas extend over 30 cm².

Results confirm the rapid tendency of the MiMS approach toward overestimation of the active surface area with increasing noise levels. We note however that the estimation is unbiased when no noise is added to the data.

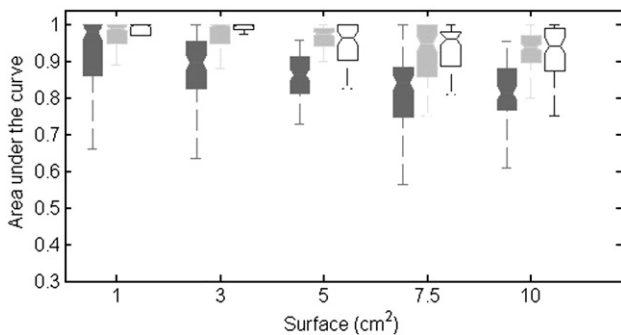


Fig. 7. Simulation of a single active region with increasing surface area (1, 3, 5, 7.5 and 10 cm²). AUC statistics for the WMNE (black), MiMS (gray) and the MiMS WMNE (white) source models. The boxplots show the AUC values for the first quartile, median, last quartile, first and last deciles of AUC indices from the Monte-Carlo samples.

Illustrative example on real data: somesthetic mapping of hand fingers

Somaesthetic mapping of limbs and fingers has been widely investigated using MEG (see e.g. Kakigi et al., 2000). The early ($t < 40$ ms) neural responses following stimulation of hand fingers for instance, follow a somatopic organization along the posterior bank of the central sulcus with the thumb area being wider, more lateral and inferior than the other fingers' (Penfield and Boldrey,

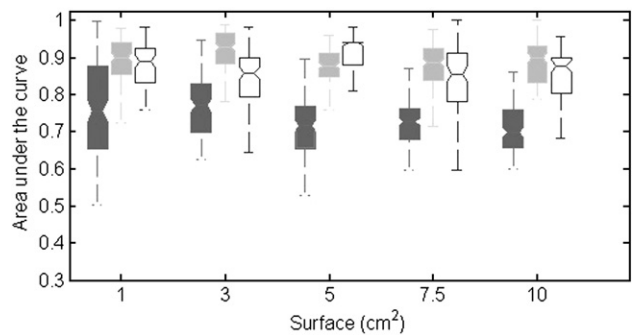


Fig. 8. Simulation of 3 activated clusters with increasing surface areas. See Fig. 7 for details on the display.

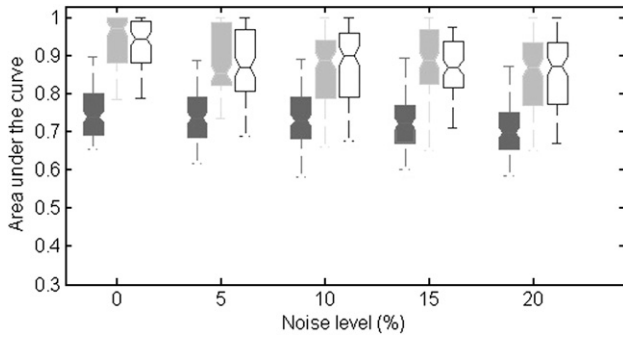


Fig. 9. Activation of multiple source regions: effects of increasing noise level. AUC boxplots from 50 simulated source sets of 3 10 cm² active regions with increasing noise levels. WMNE (black), MiMS (gray) and MiMS WMNE (white).

1937). Most somatotopic source models were restricted to ECD source models so far. Data from animal models and previous multiresolution imaging models (David and Garnero, 2002) however indicate that even though there is indeed some somatotopic organization of finger areas, these latter might be larger than expected and even overlap considerably. These findings suggest that a distributed imaging model of the primary somatotopic neural responses following stimulation of hand fingers would be more relevant than the possibly misleading focal representation of the ECD.

Data from a single subject was obtained following the random stimulation of his hand fingers with the delivery of small electric shocks below motor threshold (see Meunier et al., 2001 for a detailed description of the paradigm). Source analysis was obtained from the coupled MiMS WMNE model over a 20-ms data segment centered at about 40 ms after stimulus delivery and with the same source amplitude cut-off value as in the On the estimation of the spatial extent of activations section.

Results are summarized in Fig. 12 and indeed reveal a somatotopic organization for finger responses, with as expected, a large degree of overlap. The respective surface areas for each finger

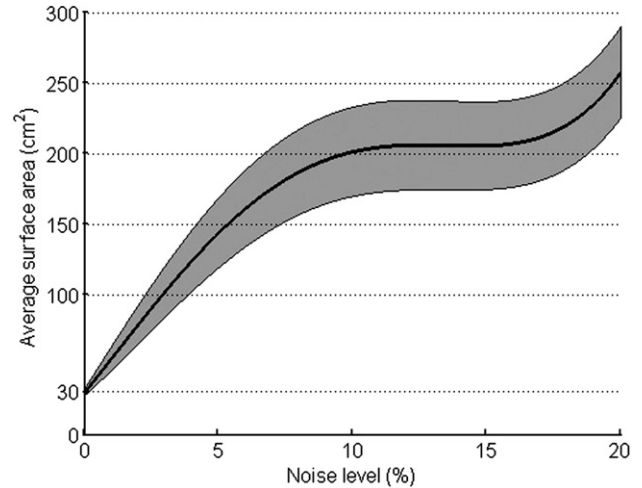


Fig. 11. Evaluation of total activated surface area: influence of noise. The solid line (resp. the gray band) is the average (resp. standard error) of total activated surface area recovered from Monte-Carlo data simulations with 3 active regions of 10 cm² each. Noise level was increased from 0% (no noise) to 20%.

were: 46 cm² (thumb), 29 cm² (index), 34 cm² (middle) and 36 cm² (little), respectively (no stimulation was delivered to the 4th finger).

Discussion and conclusions

We have introduced a new multiresolution approach to the MEG inverse problem. The procedure operates successive designs, evaluations and selections of piecewise image models as spatial resolution increases. The optimal image source model is selected retrospectively in the least GCV-error sense. Model uncertainty is evaluated empirically through the sampling of multiple initial conditions, i.e. equivalent image models at the coarsest spatial resolution.

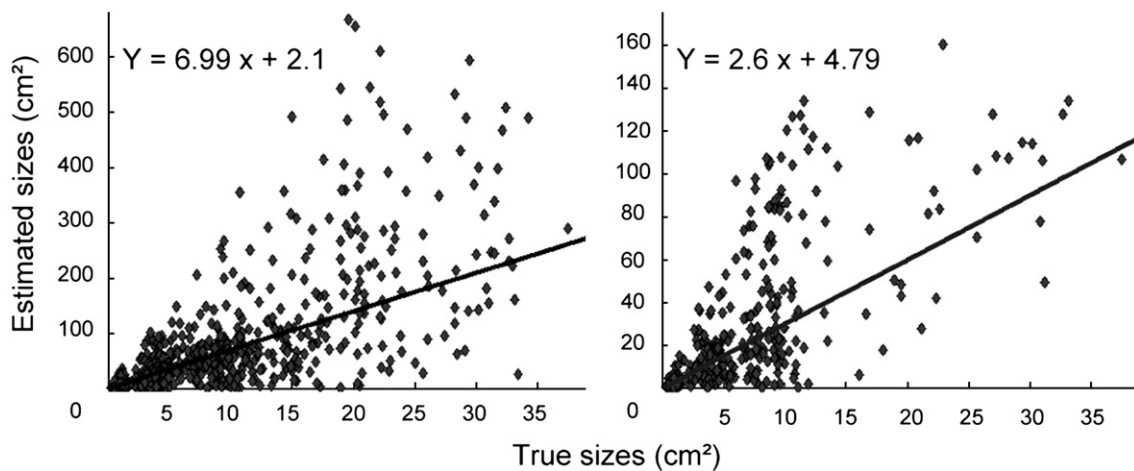


Fig. 10. True vs. estimates of the spatial extent of active surface regions, from 250 Monte-Carlo simulations of a single active region of variable size and location. Plots show the estimated surface extent obtained from MiMS (left) and MiMS WMNE (right) against the true values. The solid line in each plot is a linear fit to the Monte-Carlo simulations and suggest significant correlation with true values for both image models, with limited overestimation from the MiMS WMNE approach (see equations of the regression lines).

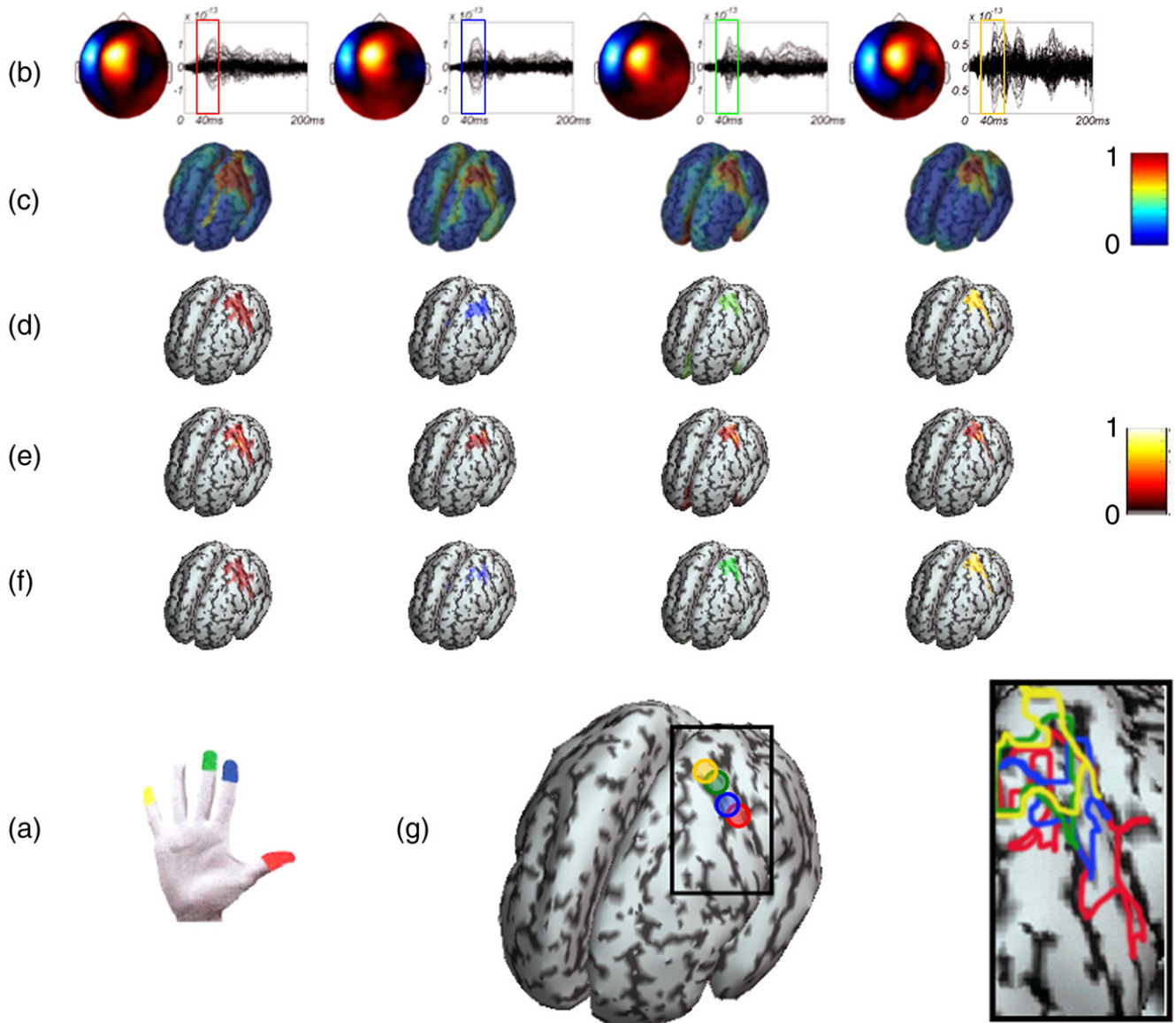


Fig. 12. Early somatotopic cortical responses of hand fingers. (a) Color-encoding of the four fingers stimulated in the study, as used in subsequent plots. (b) Butterfly time plots of the MEG time series and corresponding sensor topography of the respective brain responses following finger stimulation. Frames indicate the respective latencies on which source analysis was computed. (c) The corresponding maps \mathbf{W} of probability-like activation coefficients. (d) The MiMS image model and (e) the coupled MiMS WMNE current estimates. (f) Estimation of the respective spatial extent of the cortical responses; with (g) superposition of the corresponding contours.

This approach yields a map \mathbf{W} of empirical probability of activation for all elementary dipoles that spatially sample the cortical manifold. This map can be thresholded to select the most significant dipole sources, which conducts to the final multi-resolution image model selection (MiMS). This latter may be coupled to an image estimate of the currents which will use the coefficients from the thresholded \mathbf{W} map as intrinsic priors. We have exemplified this approach with the MiMS WMNE inverse model.

We emphasise that any other estimator of distributed source amplitudes may also be coupled to the source selection procedure. This is of particular interest when these latter are computationally demanding and result as being practically untractable when run on a high-resolution tessellations of the cortical envelope.

The MiMS procedure keeps the number of unknown free parameters constant at all spatial resolutions, which was set to the number of instantaneous data (i.e. on the order of 200). This was achieved by modelling each cortical parcel in the model by a 4th-order current multipolar expansion. We suggest that the cortical parcels of the piecewise image model can be obtained from priors of multiple anatomical and/or functional origins. This was illustrated by the usage of an atlas of Brodmann areas that was co-registered to the subject's anatomy using affine transformation. This information was complemented by the prior that the distribution of the parcel surface areas should be homogeneous at all spatial resolutions, with limited variations of curvature within each parcel. We show that automatic detection of crest lines along the gyral crowns yield efficient parcellation guidelines in that respect.

The MiMS procedure is tractable and reasonably fast (about 1 min using a 10,000-node cortical tessellation and for a data segment of arbitrary length).

Results from extensive Monte-Carlo simulations show good performances in terms of detection accuracy for the localization of up to 3 simultaneous activated regions of size up to 10 cm². The MiMS estimate is also robust to realistic noise levels in the data. The MiMS strongly overestimates the active surface area, but we have shown this effect can be dramatically reduced once the MiMS is coupled to an estimate of currents (as with the MiMS WMNE inverse model). The strong qualitative correlation with the true surface extent of active regions positively suggests that this parameter of brain activation may be extracted from MEG data in e.g. longitudinal studies.

This was exemplified on the data from the somatotopic paradigm, where the thumb's primary area was found being larger than the other fingers'. This result remains qualitative though and needs to be confirmed by the estimation of error bounds on the borders of activated regions which could readily be achieved by e.g. bootstrap approaches (Darvas et al., 2005) and extended to a group of subjects in a dedicated study.

Recent developments of multipole models for electrical potentials open perspectives for the application of the MiMS approach to EEG. Future developments might also consider an optimal approach to the analysis of long data segments where activations are likely to unfold over multiple brain areas which may not all be correctly detected from the \mathbf{W} map. The exhaustive estimation of MiMS at every time instant may be advantageously accelerated by considering the auto-correlation of MEG and EEG signals in the very estimation process.

Acknowledgments

The authors are grateful to Dr Sabine Meunier from the Laboratory Physiology and Physiopathology of Human Motricity, La Salpêtrière Hospital, INSERM, Paris, for permission to use parts of her somatosensory MEG data.

Appendix A. ROC analysis

Let i be the index of an elementary current dipole in the global image support \mathcal{D} defined on the cortical manifold Γ . The MiMS yields a map \mathbf{W} of empirical activation probabilities \bar{w}_i , and once coupled to any estimator of dipole magnitudes as with the MiMS WMNE approach produces an estimate of the distributed local current density \hat{J}_i .

In both situations, ROC analysis estimates the variation of sensitivity and specificity when either maps \mathbf{W} or \hat{J} are thresholded with a variable cut-off value, β . Sensitivity and specificity are defined from the enumeration of true/false positives/negatives in the thresholded normalized map \mathbf{W} or \hat{J} (see Eq. (16)), generically denoted $E = \{e_i, i \in \mathcal{D}\}$.

By definition, dipole d_i is:

- (1) a TP, if it is effectively active and $e_i \geq \beta$;
- (2) a FP if it is effectively inactive and $e_i \geq \beta$;
- (3) a TN if it is effectively inactive and $e_i < \beta$;
- (4) a FN if it is effectively active and $e_i < \beta$.

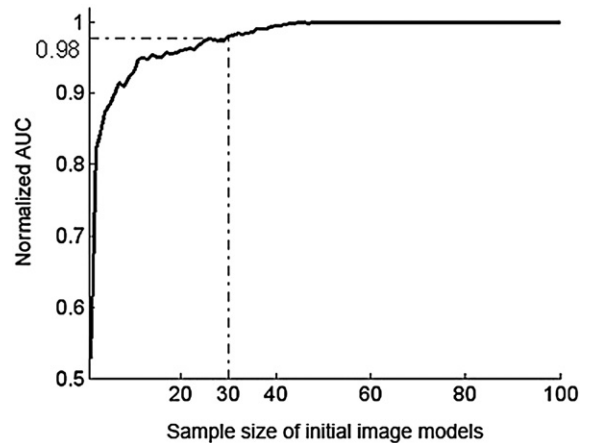


Fig. B. Evolution of the normalized AUC performances with an increasing number of samples taken as initial image models \mathcal{M}_1 . Taken at $L=30$, this metric is within 2% of its asymptotic value hence justifying this number of initial conditions in practice.

Appendix B. Model uncertainty with efficient sampling of initial conditions

We suggest the uncertainty on the optimal model in the least GCV-error sense be sampled by considering multiple instances of the initial image model \mathcal{M}_1 at the coarsest resolution. Hence, we need to determine how many samples should be considered to approach an exact estimation of model uncertainty.

We have used the data from the Monte-Carlo experiments detailed in the Evaluation procedure section to achieve the empirical estimation of L , by measuring the evolution of normalized AUC performances with an increasing number of \mathcal{M}_1 samples. The results are summarized in Fig. B for L ranging from 1 to 100.

We verified that $L=30$ is indeed a representative value where the AUC performances reach convergence.

References

- Auranen, T., Nummenmaa, A., Hämäläinen, M.S., Jääskeläinen, I.P., Lampinen, J., Vehtari, A., Sams, M., 2005. Bayesian analysis of the neuro-magnetic inverse problem with $l(p)$ -norm priors. *NeuroImage* 26 (3), 870–884.
- Baillet, S., Garnero, L., 1997. A Bayesian approach to introducing anatomic-functional priors in the EEG/MEG inverse problem. *IEEE Trans. Biomed. Eng.* 44, 374–385.
- Baillet, S., Mosher, J.C., Leahy, R.M., 2001. Electromagnetic brain mapping. *IEEE Signal Process. Mag.* 18, 14–30.
- Dale, A.M., Sereno, M.I., 1993. Improved localization of cortical activity by combining EEG and MEG with MRI cortical surface reconstruction: a linear approach. *J. Cogn. Neurosci.* 5, 162–176.
- Darvas, F., Rautiainen, M., Pantazis, D., Baillet, S., Benali, H., Mosher, J. C., Garnero, L., Leahy, R.M., 2005. Investigations of dipole localization accuracy in MEG using the bootstrap. *NeuroImage* 2 (25), 355–368.
- Dassios, G., in press. Interior Electric Potential for the Sphere with a Dipole. *Lecture Notes in Mathematics, Mathematical Biosciences*. Springer.
- Daunizeau, J., Mattout, J., Clonda, D., 2005. Bayesian spatio-temporal approach for EEG source reconstruction: conciliating ECD and distributed models. *IEEE Trans. Biomed. Eng.* 53 (3), 503–516.
- David, O., Garnero, L., 2002. Time-coherent expansion of EEG/MEG cortical sources. *NeuroImage* 17, 1277–1289.
- de Munck, B., van Dijk, J., Spekreijse, H., 1988. Mathematical dipoles are

- adequate to describe realistic generators of human brain activity. *IEEE Trans. Biomed. Eng.* 35 (11), 960–966.
- Demoment, G., 1989, Dec. Image reconstruction and restoration: overview of common estimation structures and problems. *Acoustics, Speech, and Signal Processing* [see also *IEEE Transactions on Signal Processing*]. *IEEE Trans. Signal Process.* 37 (12), 2024–2036. doi:10.1109/29.45551.
- Flandin, G., Kherif, F., Pennec, X., Riviere, D., Ayache, N., Poline, J.-B., 2002. Parcellation of brain images with anatomical and functional constraints for fmri data analysis. *IEEE International Symposium on Biomedical Imaging (ISBI'02)*, Washington, USA (URL citeseer.ist.psu.edu/flandin02parcellation.html).
- Friston, K., Henson, R., Phillips, C., Mattout, J., 2006. Bayesian estimation of evoked and induced responses. *Hum. Brain Mapp.* 27, 722–735.
- Gavit, L., Baillet, S., Mangin, J.J., Pescatore, J., Garnero, L., 2001. A multiresolution framework to MEG/EEG source imaging. *IEEE Trans. Biomed. Imag.* 48 (10), 1080–1087.
- Gorodnitsky, I.F., George, J.S., Rao, B.D., 1995, Oct. Neuromagnetic source imaging with focuss: a recursive weighted minimum norm algorithm. *Electroencephalogr. Clin. Neurophysiol.* 95 (4), 231–251.
- Grova, C., Daunizeau, J., Lina, J.-M., Bénar, C.G., Benali, H., Gotman, J., 2006. Evaluation of EEG localization methods using realistic simulations of interictal spikes. *NeuroImage* 29, 734–753.
- Hämäläinen, M., Hari, R., Ilmoniemi, R., Knuutila, J., Lounasmaa, O., 1993. Magnetoencephalography: theory, instrumentation and applications to the non-invasive study of human brain function. *Rev. Mod. Phys.* 65, 413–497.
- Jerbi, K., Mosher, J.C., Baillet, S., Leahy, R.M., 2002. On MEG forward modelling using multipolar expansions. *Phys. Med. Biol.* 47, 523–555.
- Jerbi, K., Baillet, S., Mosher, J.C., 2004. Localisation of realistic cortical activity using current multipoles. *NeuroImage* 22, 779–793.
- Kakigi, R., Hoshiyama, M., Shimojo, M., Naka, D., Yamasaki, H., Watanabe, S., Xiang, J., Maeda, K., Lam, K., Itomi, K., Nakamura, A., 2000, Aug. The somatosensory evoked magnetic fields. *Prog. Neurobiol.* 61, 495–523.
- Kay, S.M., 1993. *Fundamentals of Statistical Signal Processing: Estimation Theory*. Prentice Hall, Englewood Cliffs, NJ.
- Knösche, T.R., Berends, E.M., Jagers, H.R.A., Peters, M.J., 1998. Determining the number of independent sources of the EEG: a simulation on information criteria. *Brain Topogr.* 11, 111–124.
- Limpiti, T., Van Veen, B.D., Wakai, R.T., 2006. Cortical patch basis model for spatially extended neural activity. *IEEE Trans. Biomed. Eng.* 53 (9), 1740–1754.
- Liu, H., Schimpf, P.H., Dong, G., Gao, X., Yang, F., Gao, S., 2005, Oct. Standardized shrinking loreta-focuss (sslofo): a new algorithm for spatio-temporal EEG source reconstruction. *IEEE Trans. Biomed. Eng.* 52 (10), 1681–1691.
- Mattout, J., Pélégrini-Issac, M., Garnero, L., Benali, H., 2005. Multivariate source prelocalization (msp): use of functionally informed basis functions for better conditioning the MEG inverse problem. *NeuroImage* 26, 356–373.
- Mazziotta, J., Toga, A., Evans, A., Fox, P., Lancaster, J., Zilles, K., Woods, R., Paus, T., Simpson, G., Pike, B., Holmes, C., Collins, L., Thompson, P., MacDonald, D., Iacoboni, M., Schormann, T., Amunts, K., Palomero-Gallagher, N., Geyer, S., Parsons, L., Narr, K., Kabani, N., Le Goualher, G., Boomsma, D., Cannon, T., Kawashima, R., Mazoyer, B., 2001, Aug. A probabilistic atlas and reference system for the human brain: International consortium for brain mapping (icbm). *Philos. Trans. R. Soc. Lond., B Biol. Sci.* 356 (1412), 1293–1322 (doi:10.1098/rstb.2001.0915). URL <http://dx.doi.org/10.1098/rstb.2001.0915>.
- Metz, C.E., 1998. Statistical comparison of two ROC-curve estimates obtained from partially paired datasets. *Med. Decis. Mak.* 18, 110–121.
- Meunier, S., Garnero, L., Ducors, A., Mazières, S., Lehéry, L., du Montcel, S.T., Renault, B., Vidailhet, M., 2001. Human brain mapping in dystonia reveals both endophenotypic traits and adaptive reorganization. *Ann. Neurol.* 50 (4), 521–527.
- Moran, J.E., Bowyer, S.M., Tepley, N., 2005. Multi-resolution focuss: a source imaging technique applied to MEG data. *Brain Topogr.* 18 (1), 1–17 (doi:10.1007/s10548-005-7896-x). URL <http://dx.doi.org/10.1007/s10548-005-7896-x>.
- Mosher, J.C., Leahy, R.M., Lewis, P.S., 1999, Mar. EEG and MEG: forward solutions for inverse methods. *IEEE Trans. Biomed. Eng.* 46 (3), 245–259.
- Murakami, S., Okada, Y., 2006. Contributions of principal neocortical neurons to Magnetoencephalography (MEG) and Electroencephalography (EEG) Signals. *J. Physiol. (Lond)*. doi:10.1113/jphysiol.2006.105379.
- Nguyen, N., Milanfar, P., Golub, G., 2001a. Efficient generalized cross-validation with applications to parametric image restoration and resolution enhancement. *IEEE Trans. Imag. Proc.* 10, 1299–1308.
- Nguyen, N., Milanfar, P., Golub, G., 2001b. A computationally efficient super-resolution image reconstruction algorithm. *IEEE Trans. Imag. Proc.* 10, 57–558.
- Nolte, G., Curio, G., 2000. Current multipole expansion to estimate lateral extent of neural activity: a theoretical analysis. *IEEE Trans. Biomed. Eng.* 47 (10), 1347–1355.
- Pascual-Marqui, R.D., Michel, C.M., Lehmann, D., 1994, Oct. Low resolution electromagnetic tomography: a new method for localizing electrical activity in the brain. *Int. J. Psychophysiol.* 18 (1), 49–65.
- Penfield, W.G., Boldrey, E., 1937. Somatic motor and sensory representation in the cerebral cortex of man as studied by electrical stimulation. *Brain* 60, 389–443.
- Phillips, J., Leahy, J.C., Mosher, R.M., Timsari, B., 1997. Imaging neural activity using MEG and EEG. *IEEE Eng. Med. Biol. Mag.* 16 (3), 34–42.
- Phillips, J., Mattout, J., Rugg, M.D., Maquet, P., Friston, K.J., 2005. An empirical Bayesian solution to the source reconstruction problem in EEG. *NeuroImage* 24 (4), 997–1011.
- Reeves, S.J., Mersereau, R.M., 1992, July. Blur identification by the method of generalized cross-validation. *IEEE Trans. Image Process.* 1 (3), 301–311. URL <http://dx.doi.org/10.1109/83.148604>.
- Sato, M., Yoshioka, T., Kajihara, S., Toyama, K., Goda, N., Kawato, M., 2004. Hierarchical Bayesian estimation for MEG inverse problem. *NeuroImage* 23, 806–826.
- Schmidt, D.M., George, J.S., Wood, C.C., 1999. Bayesian inference applied to the electromagnetic inverse problem. *Hum. Brain Mapp.* 7 (3), 195–212.
- Stylianou, G., Farin, G., 2003. Crest lines extraction from 3d triangulated meshes. *Hierarchical and Geometrical Methods in Scientific Visualization*, pp. 269–281.
- Stylianou, G., Farin, G., 2004. Crest lines for surface segmentation and flattening. *IEEE Trans. Vis. Comput. Graph.* 10, 536–544.
- Tao, J.X., Ray, A., Hawes-Ebersole, S., Ebersole, J.S., 2005, May. Intracranial EEG substrates of scalp EEG interictal spikes. *Epilepsia* 46 (5), 669–676 (doi:10.1111/j.1528-1167.2005.11404.x). URL <http://dx.doi.org/10.1111/j.1528-1167.2005.11404.x>.
- Tarantola, A., 2006, August. Popper, Bayes and the inverse problem. *Nat. Phys.* 2 (8), 492–494 ISSN 1745-2473. (URL <http://dx.doi.org/10.1038/nphys375>).
- Toga, A.W., Thompson, P.M., Mori, S., Amunts, K., Zilles, K., 2006, Dec. Towards multimodal atlases of the human brain. *Nat. Rev., Neurosci.* 7 (12), 952–966 (doi:10.1038/nrn2012). URL <http://dx.doi.org/10.1038/nrn2012>.
- Trujillo-Barreto, N.J., Aubert-Vázquez, E., Valdés-Sosa, P.A., 2004, Apr. Bayesian model averaging in EEG/MEG imaging. *NeuroImage* 21 (4), 1300–1319 (doi:10.1016/j.neuroimage.2003.11.008). URL <http://dx.doi.org/10.1016/j.neuroimage.2003.11.008>.
- Wagner, M., Fuchs, M., Kastner, J., 2004. Evaluation of sloreta in the presence of noise and multiple sources. *Brain Topogr.* 16 (4), 277–280.
- Wahba, G., 1990. *Spline Models for Observational Data*. Cambridge University Press.
- Waldorp, L.J., Huizenga, H.M., Grasman, R.P.P.P., Böcker, K.B.E., de Munck, J.C., Molenaar, P.C.M., 2002. Model selection in electromagnetic source analysis with an application to vef's. *IEEE Trans. Biomed. Eng.* 49 (10), 1121–1129.
- Wang, J.Z., Williamson, S.J., Kaufman, L., 1992, Jul. Magnetic source images determined by a lead-field analysis: the unique minimum-norm least-squares estimation. *IEEE Trans. Biomed. Eng.* 39 (7), 665–675.